Geophysical Journal International

Geophys. J. Int. (2010) **183,** 1185–1198 doi: 10.1111/j.1365-246X.2010.04788.x

Spatiotemporal sampling of Sq+-induced geomagnetic responses at LEO satellite altitude for a radially conductive Earth

Mark E. Everett

Department of Geology and Geophysics, Texas A&M University, TX, USA. E-mail: everett@geo.tamu.edu

Accepted 2010 August 23. Received 2010 August 1; in original form 2010 January 14

SUMMARY

A new simulation tool is introduced for extracting Earth conductivity information from geomagnetic satellites in low Earth orbit (LEO) such as CHAMP , Swarm and potential follow-on missions. Theoretical reconstruction of spherical harmonic spectra of global universal time (UT) geomagnetic field maps is analysed. An idealized regular solar daily variation field is assumed, along with its induced counterpart from a radially stratified Earth. Solar-quiet (Sq) spectra can be reliably reconstructed from discrete time-series of measurements sampled daily within a fixed UT window. A single LEO satellite should be in orbit for at least 1 yr under quiet-time conditions to ensure accurate spectral reconstruction of an Sq geomagnetic spectrum. The length of the daily sampling window and random day-to-day variability in the Sq source strength have only minor effects on spectral reconstruction. The shape of the spectra, and spectral ratios, are independent of radial mantle conductivity. Further research employing 3-D forward modelling of induction in a laterally heterogeneous earth, with more realistic and complete external source descriptions, is advocated. The new simulation tool should prove valuable to planners of future multisatellite geomagnetic missions, as well as scientists interested in analysing and interpreting satellite induction signals.

Key words: Time series analysis; Geomagnetic induction; Satellite magnetics.

1 INTRODUCTION

Satellites in low Earth orbit (LEO) are presently being used to map the geomagnetic field in unprecedented detail (Maus *et al.* 2009; Olsen *et al*. 2009). Great progress has been made in determining spherical harmonic (SH) models of the core field including its secular variation, as well as the lithospheric magnetization field. One of the largest remaining uncertainties in geomagnetic field modelling involves characterizing the external field plus its induced contribution (Sabaka *et al.* 2004). The latter depends quite sensitively on the electrical conductivity distribution within the Earth. A detailed analysis of the induced field provides important information about the geological structure of the crust and mantle, with attendant implications for geodynamics and the nature of deep-seated geological processes (Kelbert *et al.* 2009). The induced field is driven by various electric current systems flowing in the ionosphere and the magnetosphere. These external currents are significant both at quiet times and during high levels of geomagnetic activity including storms.

The primary objective of this work is to introduce a new simulation tool, similar in spirit but much smaller in scope than the Olsen *et al.* (2006) simulator, for extracting Earth conductivity information from LEO satellites such as CHAMP , Swarm and potential follow-on missions. Herein we focus exclusively on solar-quiet (Sq) excitation of radial conductivity $\sigma(r)$ profiles. Future publications will extend the work presented here to laterally heterogeneous conductivity models incorporating the important effects of the ocean and continent distribution. It is understood that LEO satellite magnetometer data alone in principle are insufficient to recover the mantle conductivity profile from Sq variations. Satellites fly above the Sq source, and thus the Sq signals seen at satellite altitude are of purely internal origin. There is no way to separate the signals into external and internal parts, with respect to the Earth's surface, using only satellite data. For purposes of extracting mantle conductivity, additional information is required. For example, a model of the ionospheric source current distribution should be constrained as far as possible by ground observatory and space physics data.

Our attention is restricted to an idealized regular solar daily variation, or Sq field, along with its induced counterpart. All other types of geomagnetic activity such as field-aligned currents, auroral and equatorial electrojets and the magnetospheric ring current are neglected. This paper is entirely theoretical and based on a simple analytical problem: forward modelling of along-track LEO satellite measurements of the Sq field, including its induced contributions from an underlying radially stratified Earth. In particular, we construct Sq electromagnetic response spectra, including the geomagnetic element Z^{SQ} and the total field anomaly T^{SQ}, as they would be built up from a discrete time-series of measurements sampled daily within a fixed universal time (UT) window by magnetometers aboard one or more low Earth orbiting satellites. We examine hypothetically reconstructed geoelectromagnetic spectra as a function of several parameters including mantle conductivity, day-to-day

variability in Sq source strength, the number of satellites, mission duration, the length of the UT sampling window and orbital inclination and radius.

The results of this paper provide information which may prove valuable to planners of future multisatellite geomagnetic missions, as well as scientists interested in analysing and interpreting satellite induction signals.

This study considers only the two lowest $(n, m,p) = (2, 1, 1)$ and (3, 2, 2) Sq excitation modes in which (n, m) are SH degree and order representing the spatial mode while p, measured in cycles per day, is the time harmonic representing the temporal mode of the ionospheric equivalent current source. Later studies will examine laterally heterogeneous Earth induction responses to higher order (n, m, p) modes of excitation. In particular, the role of the near-surface conductance distribution on shaping the Sq geomagnetic response at LEO altitude will be examined. Eventually it is desired to invert satellite Sq signals for both the near-surface conductance distribution generated by the oceans and continents as well as conductivity of the underlying heterogeneous mantle. The simulation tool presented in this paper is a first step towards achieving that goal.

2 Sq GEOMAGNETIC INDUCTION STUDIES

The Sq field $\mathbf{B}^{SQ}$ is the regular daily geomagnetic variation observed on magnetically quiet days (Campbell 1989). It is caused by electric currents flowing in the ionosphere in response to solar heating and the attendant photoionization of atmospheric neutral atoms. The Sq field is primarily a local time phenomenon such that, at any given location on the Earth's surface, its intensity varies with the position of the Sun (Everett 2006). A complete parametrization of the external and induced Sq potential functions in terms of SHs modulated by seasonal and diurnal fluctuations is given by Sabaka *et al.* (2002, 2004).

Global SH models of the daily variation fields based on ground observatory data have been made by several authors, including Malin (1973) and Winch (1981). Olsen (1998) has developed a radial conductivity model of the mantle based on Sq and Dst (storm-time) data from selected observatories in Europe. Early Sq global induction studies, with a view to determining mantle electrical conductivity, have been carried out by Fainberg *et al.* (1990) and Schmucker (1999b).

Analyses of satellite Sq signals have now begun to appear in the literature. Turner *et al.* (2007) have constructed an hourly sequence of global UT maps of Sq total intensity based on CHAMP satellite data from 2001. They derived similar maps using the Sq SH coefficients of Malin (1973) which are based on ground observatory data acquired during the International Geophysical Years (IGY) 1957–1958. The comparison of the satellite- and ground-based UT maps is favourable despite significant differences in geomagnetic activity levels between the two epochs. This suggests that LEO satellites can detect Sq signals above their ionospheric source region. The analysis does not explicitly treat however the Sq induction signal at satellite altitude caused by electric currents flowing in the solid Earth and the oceans.

Grammatica & Tarits (2002) use a numerical algorithm based on generalized SH expansions of the geoelectromagnetic field to compute the response at satellite altitude of heterogeneous Earth conductivity models to an Sq source characterized by the three lowest spatiotemporal modes $(n, m, p) = (2, 1, 1)$, (3, 2, 2) and (4, 3, 3). Although induction at the largest length scales dominates the Earth response, internal electric currents associated with higher order (n, m) spatial modes were also found. These higher order modes are generated by lateral conductivity variations in the crust and mantle. The authors modelled the Sq satellite induction signatures of mantle conductivity structure associated with subducting slabs and mid-ocean ridge systems. They argued that the residual anomalies, after removal of the coast effect, can be detected at LEO satellite altitude.

Kuvshinov *et al.* (2007) have computed electric currents induced within a realistic 3-D earth model by Sq source excitation. The earth model consists of a realistic ocean–continent distribution overlying a radially layered mantle. The coast effect is found to dominate the Earth's Sq induction response. At satellite altitude the anomalous Z^{SQ}, or vertical geomagnetic field due to the induced component of the Sq field, is predicted to be as much as 50 per cent of the total Sq field. Overall, the modelling results indicate that LEO satellite

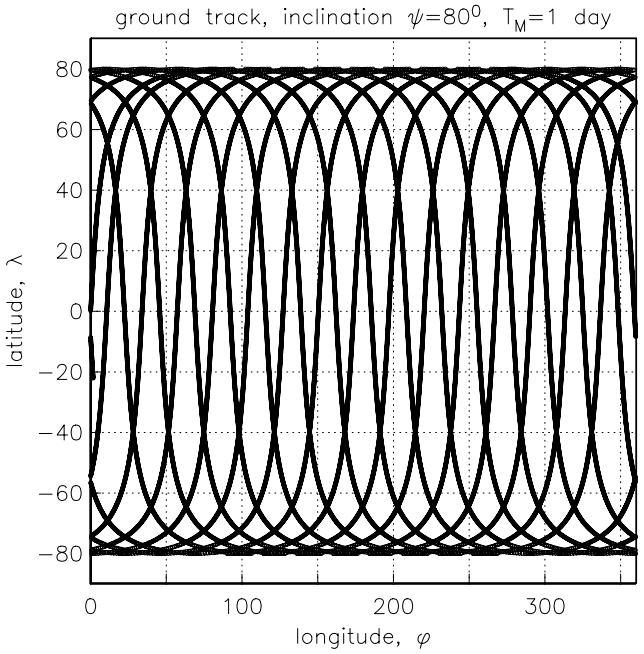

Figure 1. Ground track of an LEO satellite.

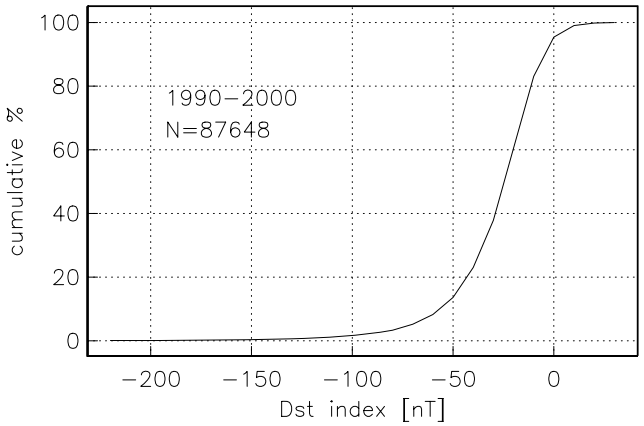

Figure 2. Dst index for the years 1990–2000. Ring current strength increases to the left on the plot abscissa. For a given Dst index level, the cumulative percentage of time between 1990–2000 for which the ring current is at least that strong can be read on the plot ordinate.

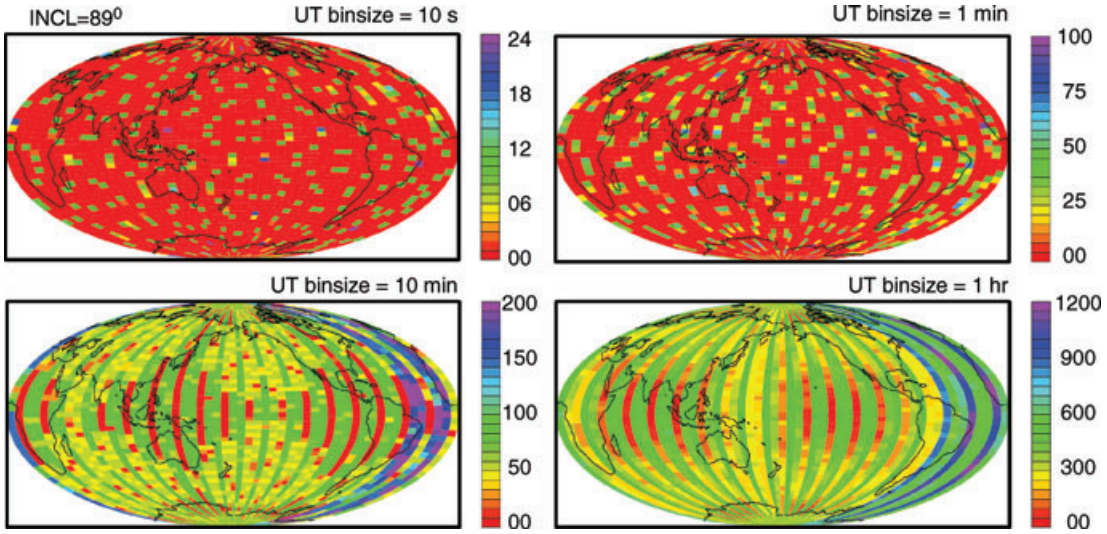

Figure 3. The number of satellite observations of the geomagnetic field for a satellite mission of 1-yr duration with near-polar orbital inclination of $\Psi = 89^\circ$. The satellite samples the geomagnetic field at 1 Hz rate each day about the prescribed UT hour for a length of time equal to twice the UT binsize. The case shown here corresponds to sampling at UT midnight and 55 longitude and 55 latitude bins.

Table 1. Canonical sampling parameters.

Parameter	Symbol	Canonical value
Mission duration	T_M	1 yr
Temporal sampling bin size	UT binsize	1 hr
Orbit inclination	Ψ	80°
No. of latitude/longitude bins	NLAT,NLON	55
Universal time	UT	0000
Orbital altitude	a	400 km

Table 2. Canonical Earth conductivity parameters.

Parameter	Symbol	Canonical value
Upper-mantle conductivity	σ_1	0.1 S m^{-1}
Mid-mantle conductivity	σ_2	0.01 S m^{-1}
Lower-mantle conductivity	σ_3	0.1 S m^{-1}
Crustal layer thickness	h_1	100 km
Upper-mantle thickness	h_2	660 km

Table 3. Canonical source parameters.

Parameter	Symbol	Canonical value
(2, 1) mode source strength	SQ(2, 1)	25.0 nT
(3, 2) mode source strength	SQ(3, 2)	−0.1 nT

magnetometer data are very sensitive to the distribution of oceans and continents.

Velímsky & Everett (2005) have also demonstrated that satellite Sq induction signals are highly sensitive to lateral heterogeneities in crustal electrical conductivity. The authors used the 3-D forward modelling code of Velímsky & Martinec (2005) with Sq as the source field to fit ground observatory and satellite residuals with a nominal three-layer mantle model. Incorporation of the near-surface conductance distribution associated with the oceans and continents improved the fit of the ground data by an average of 15 per cent, especially at coastal stations, and improved the fit of satellite data by a similar amount, especially over the oceans.

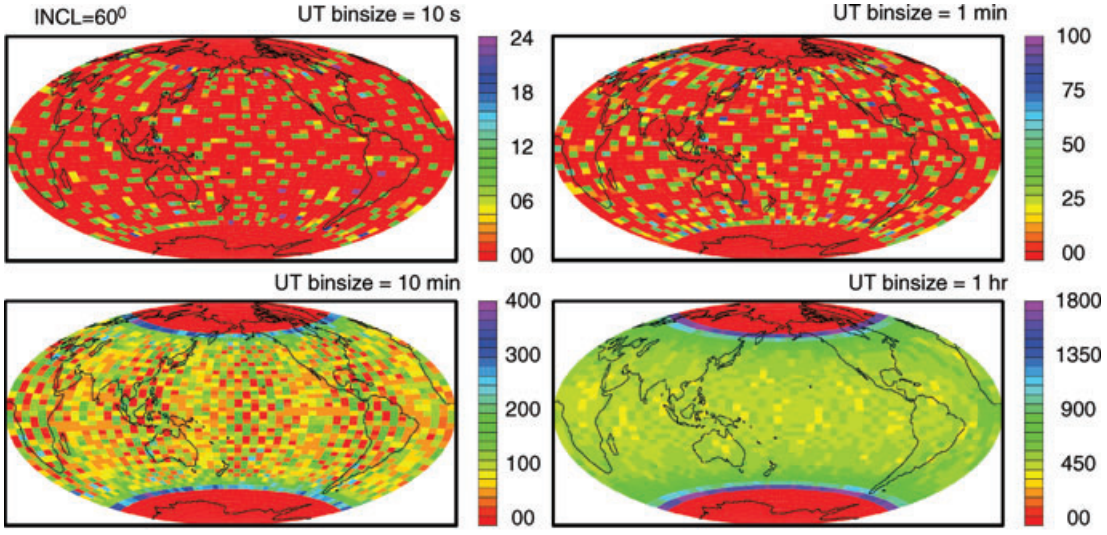

Figure 4. As in the previous figure, except for a satellite orbital inclination of $\Psi = 60^\circ$.

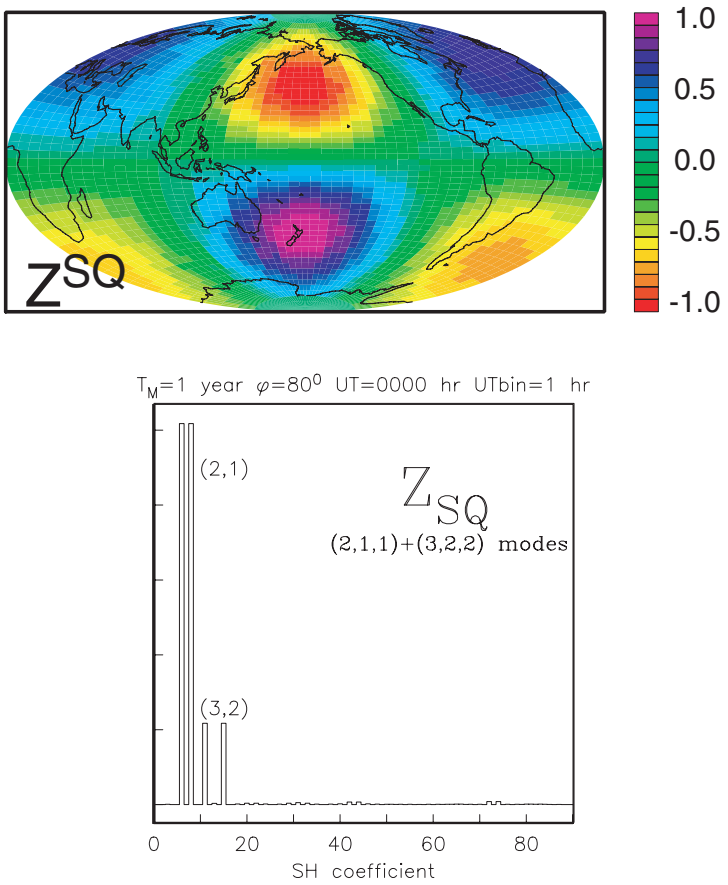

Figure 5. Map (top panel) and reconstructed SH spectrum (bottom panel) of the LEO-sampled Sq+-induced geomagnetic Z^{SQ} element for the canonical sampling parameters, Earth conductivity model and Sq source parameters listed in Tables 1–3, respectively.

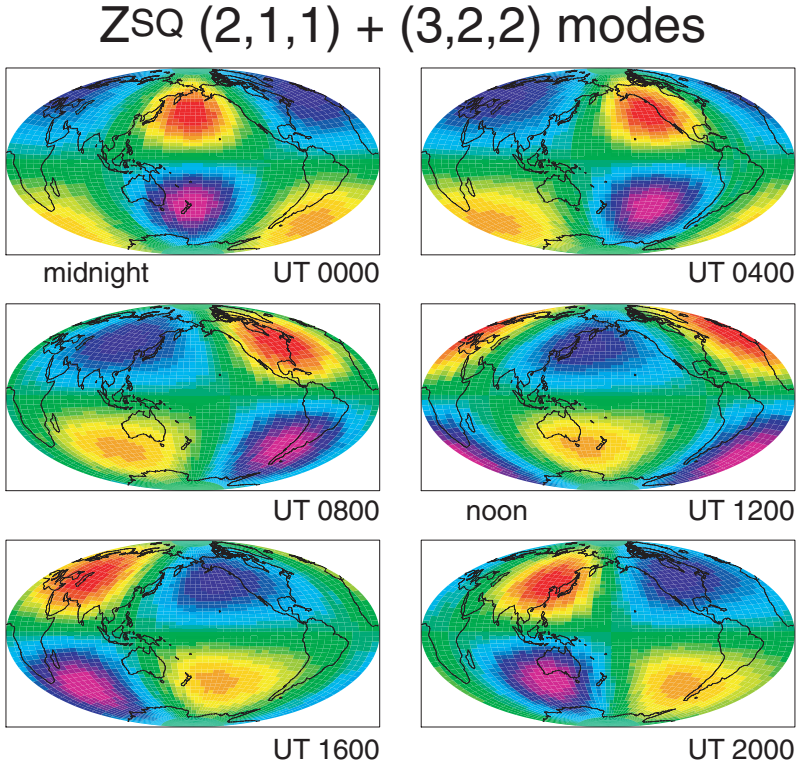

Figure 6. The UT dependence of the LEO-sampled geomagnetic Z^{SQ} element for the canonical sampling, Earth conductivity and Sq source parameters.

3 SPATIOTEMPORAL SAMPLING OF THE $\mathbf{B}^{SQ}$ GEOMAGNETIC FIELD

The analysis of satellite Sq induction signals must take into account the spatiotemporal sampling of the $\mathbf{B}^{SQ}$ field. Although the ground magnetic observatory network offers continuous temporal but sparse and irregular spatial coverage, the spatial and temporal sampling by satellites is folded together in a complicated manner. Salby (1982) and Willis & Bresler (1997) among others have discussed the theoretical information content of spatiotemporal signals subjected to time-sequential sampling.

In this paper we simulate vector and scalar magnetometer measurements aboard an LEO satellite platform in a circular orbit at altitude a. The orbital trajectory equations (Shin & North 1988) for latitude $\lambda(t)$ and longitude $\phi(t)$ as a function of time t are given in Appendix A. To illustrate a typical LEO sampling pattern, the satellite ground track for a mission duration of $T_M = 1$ d with (near-polar) orbital inclination of $\Psi = 80^\circ$ is shown in Fig. 1.

The mission duration T_M defined herein corresponds to the length of time that the LEO satellite flies under quiet-time conditions, plus those storm times for which the contributions to the geomagnetic field from an energized magnetospheric ring current, along with its induced component, have been taken into account. The hourly Dst index (Sugiura 1964) is a standard although simplified measure of the magnetospheric ring current strength. The threshold geomagnetic activity level for determining whether quiet-time conditions prevail at a given time is somewhat arbitary (Everett 2006), although for our purposes the size of the Dst index can provide a rough guide. Shown in Fig. 2 is a plot of the strength of the Dst index for the years 1990–2000, based on data from the World Data Center for Geomagnetism, Kyoto (wdc.kugi.kyoto-u.ac.jp). Ring current strength increases to the left on the plot abscissa. For a given Dst index level, the cumulative percentage of time between 1990–2000 for which the ring current is at least that strong can be read on the plot ordinate. Thus, if a Dst index threshold of –50 nT is selected as representative of quiet-time conditions then, according to the plot, storm times prevailed for ~15 per cent of the time during the decade 1990–2000. In this case, a mission duration of 1 yr under quiet-time conditions corresponds to a total flight time of 1.15 yr.

Herein we simulate an LEO satellite that reports a series of 1 Hz measurements of the ambient geomagnetic field each day for a prescribed interval of time, twice the UT binsize, centred on a specified hour of UT. Individual measurements are then assigned to a latitude and longitude bin corresponding to the instantaneous geographic location of the satellite. At the end of the mission, the data points within each bin are averaged. In this way, a UT map (as in Turner *et al.* 2007) of the geomagnetic field is built up from the daily data streams.

As an example, Fig. 3 shows the spatial sampling pattern after 1 yr in orbit for UT binsizes of 10 s, 1 min, 10 min and 1 hr. Throughout this paper, unless otherwise specified, the various satellite sampling parameters are fixed to their canonical values as indicated in Table 1. For comparison, Fig. 4 shows the spatial sampling pattern for satellite inclination $\Psi = 60^\circ$, all other parameters fixed as above.

4 RECONSTRUCTION OF Sq GEOMAGNETIC ELEMENT SPECTRA

In this section we evaluate the SH spectra of UT maps of various Sq geomagnetic field elements, as sampled by the canonical LEO satellite. Of course, these are theoretical spectra based on idealized scenarios, but spectra broadly similar to these should be observed by an actual LEO satellite mission. By convention, the north, east and vertical (downward) components of the geomagnetic field **B** are, respectively, denoted as X, Y and Z (Blakely 1995). The intensities of the Sq contributions are therefore denoted herein as X^{SQ}, Y^{SQ} and Z^{SQ}. The formula to compute the SH spectral coefficients $\overline{f}_{nm}$ from equally spaced samples of a function $f(\theta, \phi)$ defined on a sphere is given in Appendix B.

A complete derivation of the total (Sq+-induced) geomagnetic field $\mathbf{B}^{SQ}$ at satellite altitude for a layered Earth is given in Appendix C. For the calculations in this paper, except as noted, we use a three-layer mantle conductivity model with a resistive mid-mantle, as described in Table 2. The Sq source is presumed to consist only of diurnal $p = 1$ and semidiurnal $p = 2$ spatiotemporal modes $(n, m, p) = (2, 1, 1)$ and $(3, 2, 2)$. The mode amplitudes, except as noted, are listed in Table 3. There is no day-to-day, seasonal or other temporal variability superimposed on the Sq mode amplitudes, except as noted.

Under the assumption that at LEO satellite altitudes the magnetic field can be expressed via the gradient of the magnetic potential,

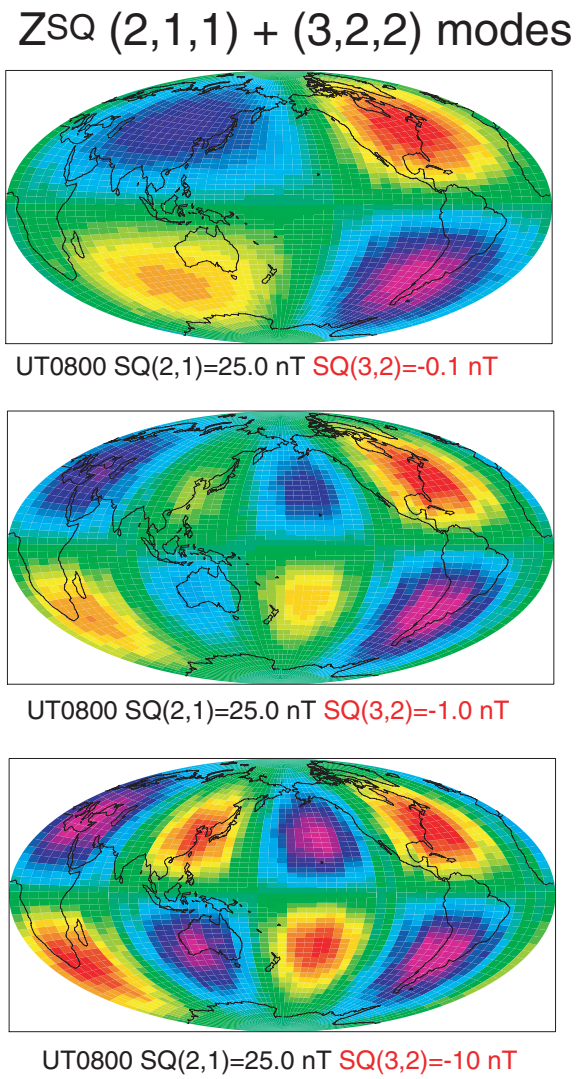

Figure 7. The effect of Sq source structure on the LEO-sampled geomagnetic Z^{SQ} element at UT 0800 hours.

as in eq. (C18), the X^{SQ}, Y^{SQ} and Z^{SQ} elements are related to the geomagnetic field $\mathbf{B}^{SQ}$ as follows:

$$X^{SQ} = -\mathbf{B}_{\theta}^{SQ} = \frac{\mu_0}{r}\frac{\partial U}{\partial \theta}; \tag{1}$$

$$Y^{SQ} = \mathbf{B}_{\phi}^{SQ} = -\frac{\mu_0}{r \sin\theta}\frac{\partial U}{\partial \phi}; \tag{2}$$

$$Z^{SQ} = -\mathbf{B}_{r}^{SQ} = \frac{\partial U}{\partial r}. \tag{3}$$

Note that X^{SQ}, Y^{SQ} and Z^{SQ} are derived from the potential U so that all three can be described using a single set of SH coefficients, U_{nmp}. The three geomagnetic elements are therefore not independent scalar variables. Moreover, from eqs (1) and (2) it is evident that the X^{SQ} and Y^{SQ} elements are naturally expanded in terms of spatial derivatives of surface harmonics $P_{nm}(\cos\theta)\exp(\mathrm{im}\,\phi)$, rather than the surface harmonics themselves. The Z^{SQ} element is naturally expanded in surface harmonics since it involves only a radial derivative. For a sufficiently long satellite mission, the Z^{SQ} spectral peaks should correspond only to the degrees and orders that are actually present in the Sq source function.

The canonical UT midnight Z^{SQ} map is shown in Fig. 5 (top panel) while the reconstructed SH spectrum appears in Fig. 5 (bottom panel). The SH coefficients are enumerated in the plot abscissa as $k = n(n + 1) + m + 1$. The spectral peaks are normalized to the largest peak and are labelled by their (n, m) values. The Z^{SQ} spectrum is simple, as expected, with only the (2, 1) and (3, 2) spatial modes being of significant amplitude. There is a small broadband noise component that reflects the finite UT temporal and latitude/longitude spatial binning.

It is well-known that the Sq field is primarily a local-time phenomenon. At any given mid-latitude geographic location, the overhead current system, and hence the regular daily geomagnetic variation, is strongest at local noon and during the early afternoon. The Sq field strength diminishes considerably towards the late evening and during the nighttime. In Fig. 6 is plotted a series of UT maps of the canonically sampled Z^{SQ} geomagnetic element. A UT map for a specific hour can be considered as the equivalent local-time map at Greenwich. Note that the strongest signals at UT noon (middle right panel) are found, as expected, above the

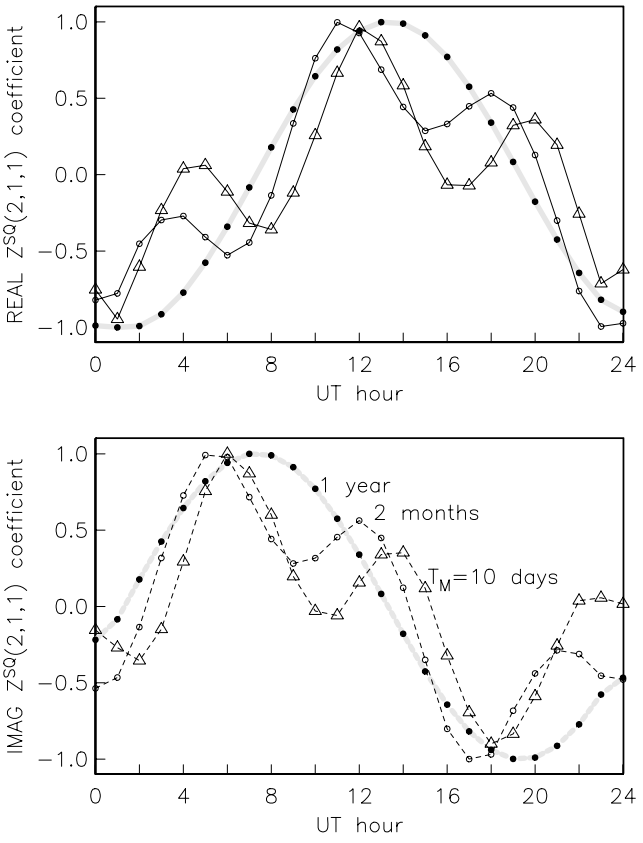

Figure 8. (Top panel) The real part of the reconstructed Z^{SQ} (2, 1, 1) mode coefficient as a function of universal time. The triangles correspond to mission duration $T_M = 10$ d; the open circles to $T_M = 2$ months and the solid circles to $T_M = 1$ yr. The thick grey line is an ideal diurnal variation. (Bottom panel) The imaginary part of the reconstructed Z^{SQ} (2, 1, 1) mode coefficient as a function of universal time.

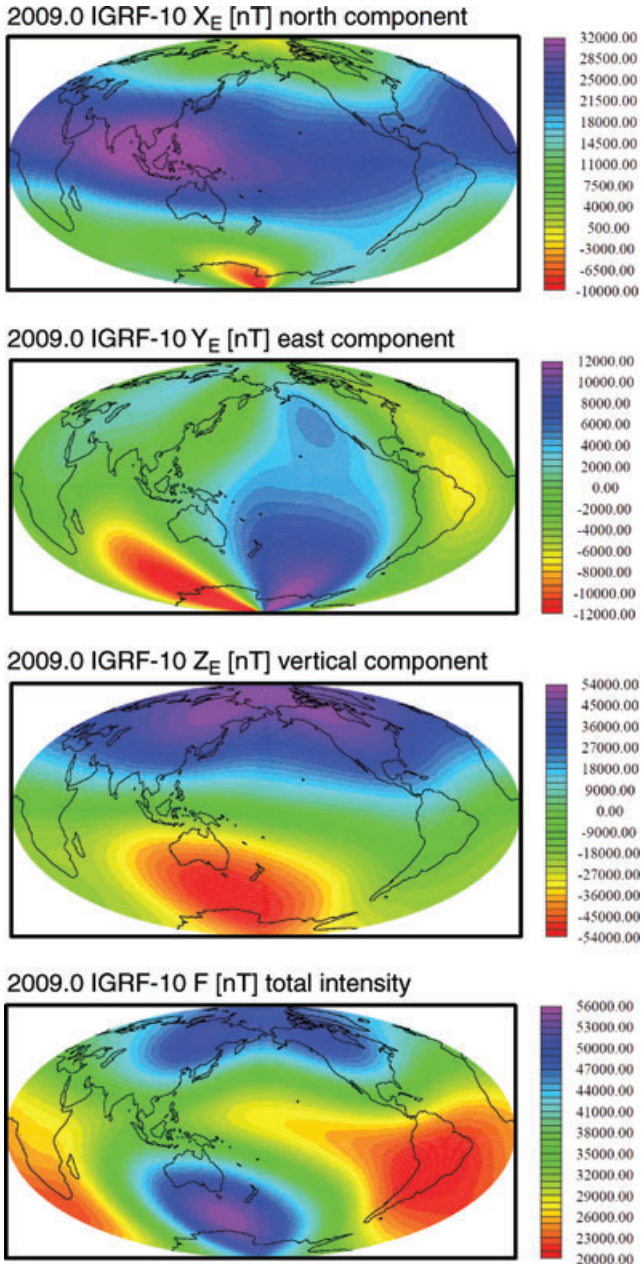

Figure 9. The IGRF–10 geomagnetic field model of Macmillan & Maus (2005).

Greenwich meridian. Weak signals at Greenwich, but stronger signals above the central Pacific Ocean, are found at UT midnight (top left panel). This is also expected since in the central Pacific Ocean the Sun is directly overhead at UT midnight. In general, the spatial pattern of Z^{SQ}, and the other elements X^{SQ} and Y^{SQ} (not shown), are Sun-synchronous. The apparent diurnal variation seen in Fig. 6 is caused by the rotation of Earth under the daytime Sq current vortices.

The effect of varying the Sq source field on the Z^{SQ} geomagnetic element at LEO satellite orbit is shown as a series of UT0800 (morning at Greenwich) maps in Fig. 7. The top panel repeats the canonical result presented in the previous figure. The middle panel and lower panel show results for progressively stronger (3, 2, 2) mode amplitudes, 1.0 nT and 10 nT, respectively. The fundamental (2, 1, 1) mode amplitude is held fixed at 25.0 nT. As expected, the complexity of the Z^{SQ} spatial pattern increases as the amplitude of the higher order (3, 2, 2) mode increases relative to the fundamental (2, 1, 1) mode.

The SH coefficients have been evaluated separately for different UTs. However, the diurnal (semi-diurnal, and so forth) time periodicity of the presumed Sq variations is not recovered in the analysis. To illustrate the capability of LEO satellite data to resolve temporal variability of the Sq geomagnetic field, in Fig. 8 is shown the reconstructed Z^{SQ} (2, 1, 1)-mode coefficient as a function of UT. Note that the diurnal variation is clearly recovered for the canonical case of a satellite mission of 1 yr in duration. If the mission is of briefer duration, such as 2 months or 10 d, as shown in the figure the diurnal periodicity is poorly recovered due to incomplete spatiotemporal sampling.

5 RECONSTRUCTION OF Sq GEOMAGNETIC TOTAL-FIELD ANOMALY SPECTRA

It is traditional in crustal-scale magnetic prospecting to construct the total field anomaly T from scalar intensity data. The total field anomaly is defined as the difference between the measured intensity $\mathbf{B}^{OBS}$ and the intensity of the ambient geomagnetic field $F = |\mathbf{B}^{E}|$, that is, $T = |\mathbf{B}^{OBS}| - F$. It is readily shown (Blakely 1995) that, for $|\mathbf{B}^{SQ}| \ll F$,

$$T^{SQ} \approx \mathbf{B}^{SQ} \cdot \hat{\mathbf{B}}^{E} = (X^{SQ}X^{E} + Y^{SQ}Y^{E} + Z^{SQ}Z^{E})/F, \quad (4)$$

where it has been assumed that $\mathbf{B}^{OBS} = \mathbf{B}^{E} + \mathbf{B}^{SQ}$. In other words, the observed magnetic field is considered to be the sum of the ambient geomagnetic field $\mathbf{B}^{E}$, describing mainly core and lithospheric contributions, plus the Sq field $\mathbf{B}^{SQ}$. The total field anomaly, as

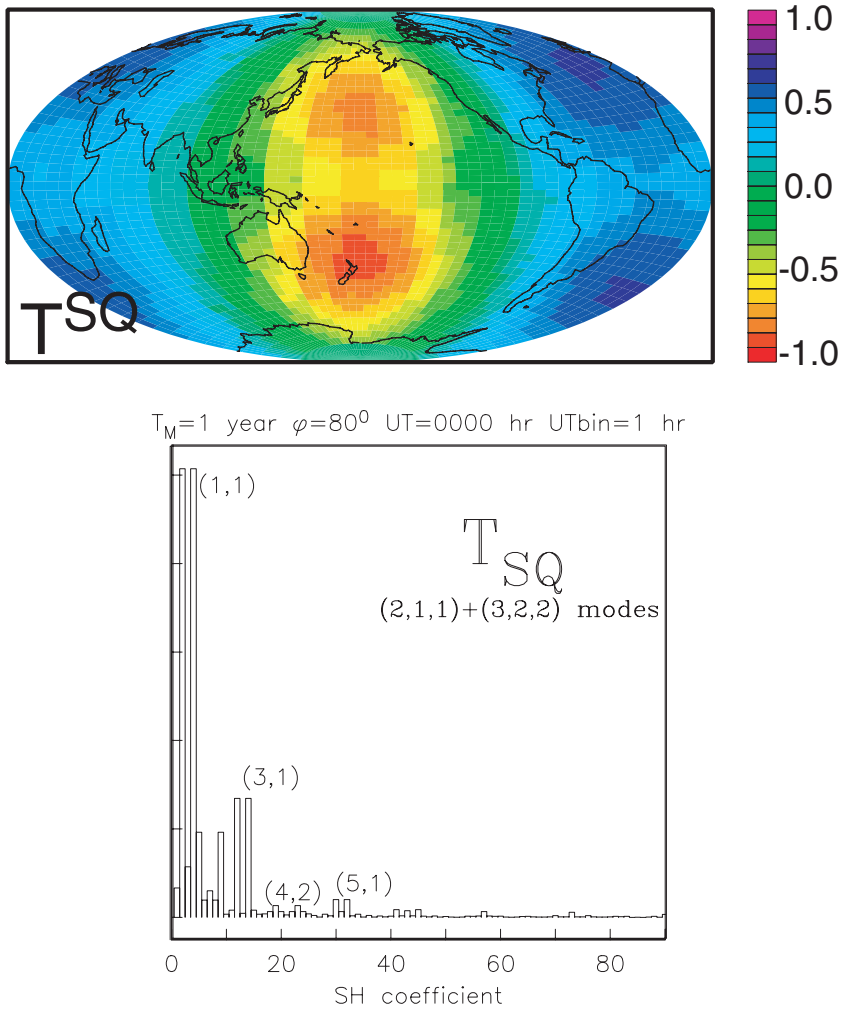

Figure 10. Map (top panel) and reconstructed SH spectrum (bottom panel) of the LEO-sampled Sq+-induced geomagnetic total field anomaly T^{SQ} for the canonical sampling parameters, Earth conductivity model and Sq source parameters listed in Tables 1–3, respectively.

indicated in eq. (4), is simply the projection of the Sq field into the direction of the ambient geomagnetic field. For this paper we assign $\mathbf{B}^{\mathrm{E}}$ as the IGRF–10 geomagnetic field model of Macmillan & Maus (2005). The IGRF–10 geomagnetic field elements X^{E}, Y^{E}, Z^{E} and the intensity F are shown in Fig. 9. The total field anomaly T^{SQ} is relatively straightfoward to compute from satellite scalar intensity data (Turner *et al.* 2007) and is insensitive to satellite attitude errors.

The UT map for the Sq total field anomaly T^{SQ} is shown in Fig. 10 (top panel). The T^{SQ} map is computed from the canonically sampled $\mathbf{B}^{\mathrm{SQ}}$ field using eq. (1) along with IGRF–10. Note that the largest signals for the UT midnight map are located over the central Pacific Ocean, where the Sun is directly overhead. This is in agreement with the findings of Turner *et al.* (2007). The reconstructed SH spectrum appears in Fig. 10 (bottom). The T^{SQ} spectral signature is dominated by the (1, 1) and (3, 1) spatial patterns, as shown, with smaller contributions from modes (2, 2), (4, 2) and (5, 1).

The SH spectra that have been presented in this paper so far correspond to the canonical sampling and Earth conductivity parameters. In the next series of plots these parameters are systematically varied. In Fig. 11, for example, the effect on the T^{SQ} spectrum of varying the satellite mission duration is shown. The canonical spectrum for mission duration $T_{\mathrm{M}} = 1$ yr is shown at the bottom right-hand panel. This is the asymptotic spectrum; it does not change appreciably for longer mission durations. However, if the mission duration is brief, as at the top left-hand panel for which $T_{\mathrm{M}} = 1$ d, the T^{SQ} spectrum is very noisy with many spurious peaks evident across the wavenumber spectrum. The noisy spectrum is a consequence of an incomplete sampling of the complete set of latitudes and longitudes by the satellite during a short mission. It is essentially an aliasing phenomenon. As the mission duration increases from $T_{\mathrm{M}} = 1$ week (top right-hand panel) to $T_{\mathrm{M}} = 1$ month (bottom left-hand panel), the T^{SQ} spectrum converges steadily to its canonical value. This result indicates that an LEO satellite should be in orbit for at least 1 yr to ensure accurate reconstruction of the T^{SQ} spectrum from the geomagnetic field samples.

The effects on the T^{SQ} spectrum of varying the UT binsize is shown in Fig. 12. Recall that twice the UT binsize is the length of the daily data sampling window centred on the specified UT hour. Geomagnetic field measurements are reported by the satellite at a 1 Hz sampling rate. Thus, a UT binsize of 1 hr implies that 7200 geomagnetic field measurements are reported each day and placed into the appropriate latitude/longitude bins. The canonical spectrum with UT binsize = 1 hr is shown at the bottom right-hand panel. The other plots in this figure show T^{SQ} spectra for UT binsizes of 1 s,

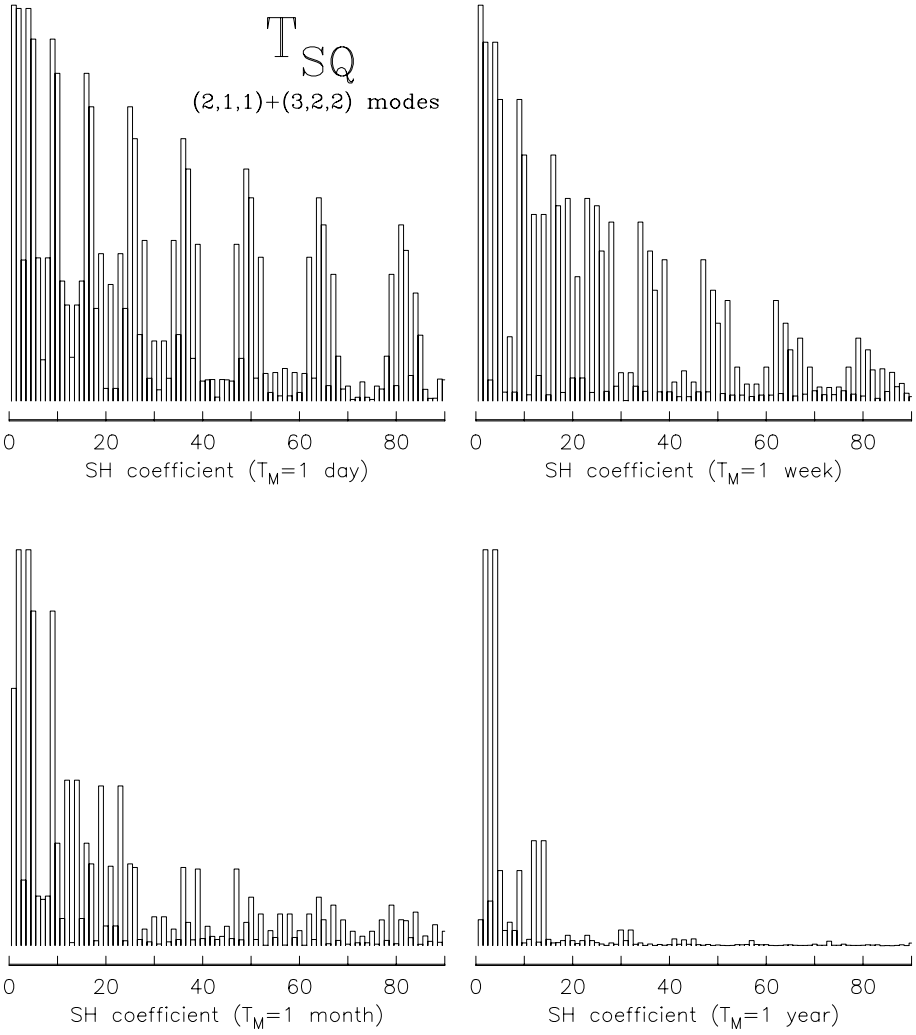

Figure 11. Effect of varying satellite mission length on the reconstructed SH spectrum of the geomagnetic total field anomaly T^{SQ}.

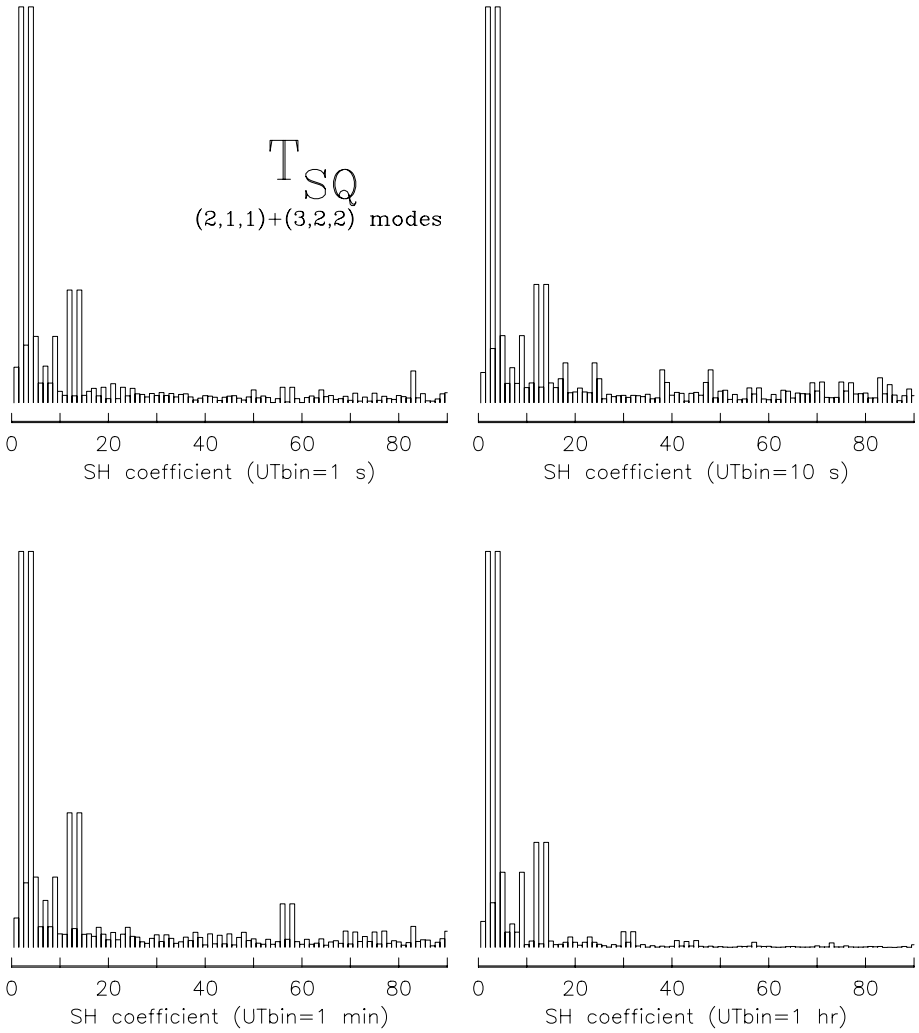

Figure 12. Effect of varying UT sample binsize on the reconstructed SH spectrum of the geomagnetic total field anomaly T^{SQ}.

10 s and 1 min. The major peaks in the spectrum do not appear to depend on the UT binsize. However, the amplitude of the noise continuum is larger for the smaller UT binsizes. Clearly this indicates a trade-off between UT binsize and the spectral noise. As the UT binsize increases, there is proportionately more temporal averaging inherent in building the UT map. This does not seem to negatively affect the spectrum. Although the length of the daily sampling window does not have a major effect on spectral reconstruction for the layered Earth presently under consideration, the presence of lateral conductivity heterogeneities, which should generate significant higher order (n, m) spatial modes, will likely change that situation.

The day-to-day variability of the Sq geomagnetic field is significant and should also be taken into account in satellite induction studies. The causes of the variability are fluctuations in source intensity and shifts in the location of the Sq current foci (Stening *et al.* 2005; Chen *et al.* 2007) due to solar wind and atmospheric phenomena. Herein we model the effects on the T^{SQ} spectrum of day-to-day variability simply as a Gaussian-distributed random number added to the canonical (2, 1) mode source strength given in Table 3. The results are shown in Fig. 13. The top left panel shows again the canonical spectrum with no day-to-day variability. The other three plots show the reconstructed T^{SQ} spectrum with 2 per cent, 5 per cent and 10 per cent daily random Gaussian noise added to the canonical (2, 1)-mode source strength. It is readily seen that the addition of random day-to-day variability in the Sq source strength has little effect on the T^{SQ} spectral reconstruction, for the idealized layered earth model under consideration. The results are encouraging in the sense that random day-to-day fluctuations in the Sq source intensity appear unlikely to prohibitively impact determinations of Earth conductivity from satellite data.

6 EFFECTS OF EARTH CONDUCTIVITY AND MULTIPLE SATELLITES

It is well known that an external current source with (n, m) spatial structure flowing in a thin radial shell excites only the (n, m) in a 1-D earth characterized by radial conductivity profile $\sigma(r)$. Higher order modes are generated by lateral heterogeneities in the Earth's conductivity structure, as noted by several authors including Grammatica & Tarits (2002) and Kuvshinov *et al.* (2007). Thus, although we expect the magnitude of the SH spectral coefficients of the various Sq geomagnetic elements to vary with the underlying 1-D radial conductivity model, we do not expect to see a change in shape of the spectra. This is borne out in Fig. 14. The plot shows the change in the amplitude of the (2, 1)-mode coefficient of the canonical Z^{SQ}

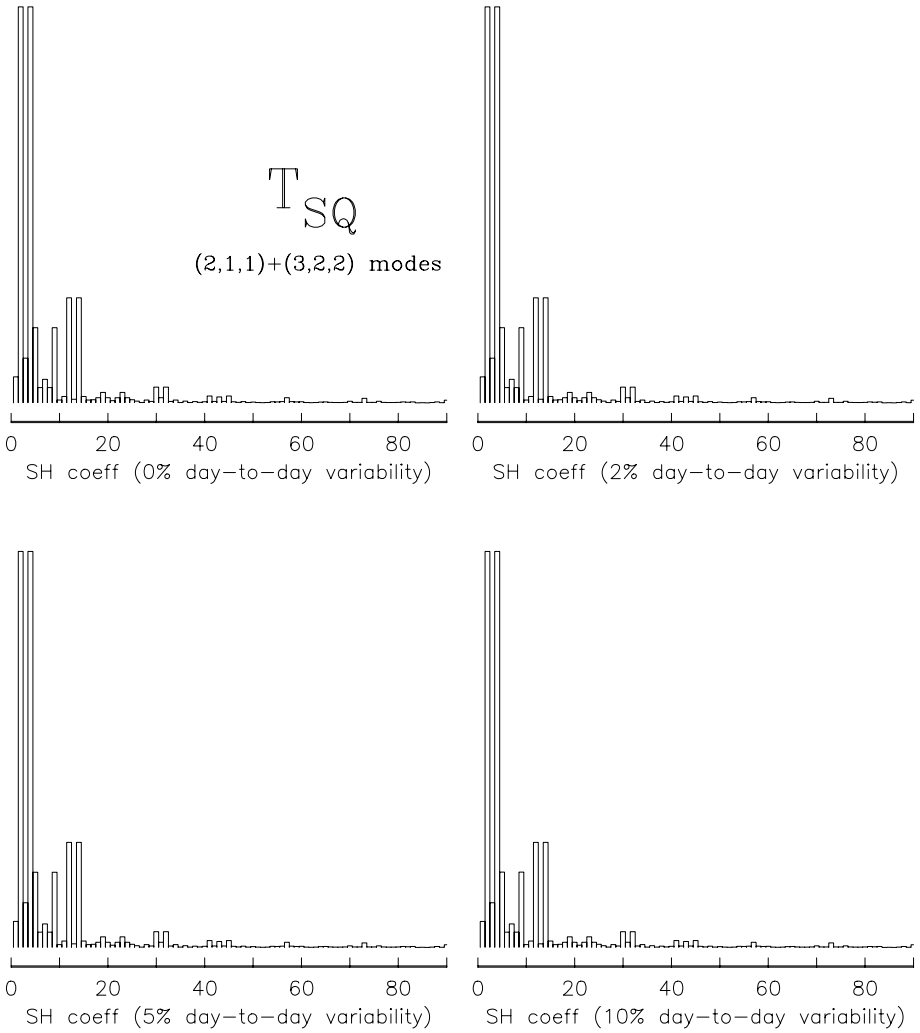

Figure 13. Effect of varying the magnitude of the day-to-day Sq source variability on the reconstructed SH spectrum of the geomagnetic total field anomaly T^{SQ}.

spectrum (see Fig. 5) as the mid-mantle conductivity is varied. It is evident that the geomagnetic Z^{SQ} (2, 1) response increases as mid-mantle conductivity is increased from 0.01 to 1.0 S m^{-1}. This is not surprising since Sq responses at the diurnal period and harmonics are sensitive to mid-mantle structure, according to the skin effect. The skin depth of geomagnetic fluctuations with a characteristic 1 d period into a uniform medium of 0.1 S m^{-1} conductivity is ∼500 km. The greater the mantle conductivity, the greater the induced current density closer to the Earth's surface, and consequently the greater the associated Sq geomagnetic response. It is also evident, as noted in the figure, that geomagnetic spectral ratios such as Z^{SQ}/T^{SQ} and X^{SQ}/T^{SQ} do not depend on mantle conductivity. They have the fixed values shown in the figure. Thus, spectral ratios cannot be used to determine the conductivity of a layered earth. However, it is anticipated that the spectral ratios will change significantly in the presence of lateral conductivity heterogeneities.

As mentioned above, the simulation tool described in this paper can be utilized to help design future multisatellite geomagnetic missions such as follow-ons to Swarm. An arbitrary number of satellites in arbitrary LEO orbits can be modelled. Herein we explore the possibilities by modelling the improvements in geomagnetic Sq spectral reconstruction that are afforded if a second LEO satellite is available.

Shown in Fig. 15 is the convergence of the (1, 1) SH coefficient of the T^{SQ} spectrum (see Fig. 10) towards its canonical value as a function of mission duration, T_M. The black curve illustrates the canonical single-satellite case; see Fig. 11 for the detailed spectrum evolution. Each of the curves in Fig. 15 is labelled by the number of satellites (N_{SAT}) and the orbital inclinations of each satellite. The remaining curves in Fig. 15 show the effects of a second satellite at inclinations of 45° (green), 60° (red) and 75° (blue). The results indicate that the second satellite should be inclined at ∼60° to achieve the fastest convergence to the canonical T^{SQ} spectrum. This type of information should prove very useful to mission designers.

The effect of varying the orbital radius of the second satellite (inclined at 60°) is shown in Fig. 16. The best results (black curve) are obtained for a radius of 300 km, that is, lower than the canonical radius of 400 km. Intermediate results are found when both satellites occupy the canonical radius (red curve). The slowest convergence to the canonical T^{SQ} spectrum is found when the second satellite is placed in a higher orbit of 600 km (green).

7 DISCUSSION AND CONCLUSIONS

This paper has introduced a new simulation tool for modelling Sq satellite induction data. An idealized scenario has been considered

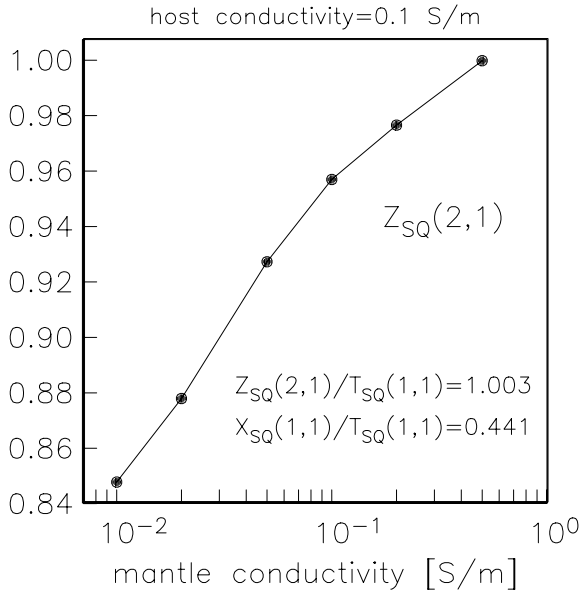

Figure 14. Effect of mantle electrical conductivity on the reconstructed SH (2, 1) spectral coefficients.

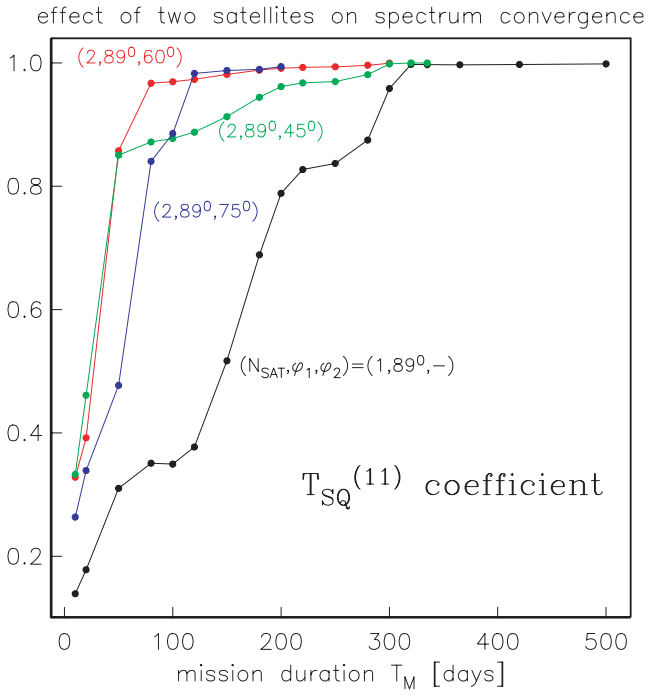

Figure 15. Effect on the SH spectral reconstruction of the geomagnetic T^{SQ} element of adding a second LEO satellite at various orbital inclinations.

in which the source is represented as the superposition of (2, 1, 1) and (3, 2, 2) spatiotemporal modes and the Earth is radially stratified with a resistive mid-mantle. All computations in this paper are based on the analytic formulae presented in the three appendices. Satellite geomagnetic measurements were herein reduced to the form of SH spectra of global UT maps of Sq geomagnetic elements. This format proved convenient for this study but it may or may not be optimal for the eventual inversion of actual satellite induction data in the presence of the laterally heterogeneous Earth. Spectral ratios of geomagnetic field elements in that case should have a rich information content from which important lateral electrical

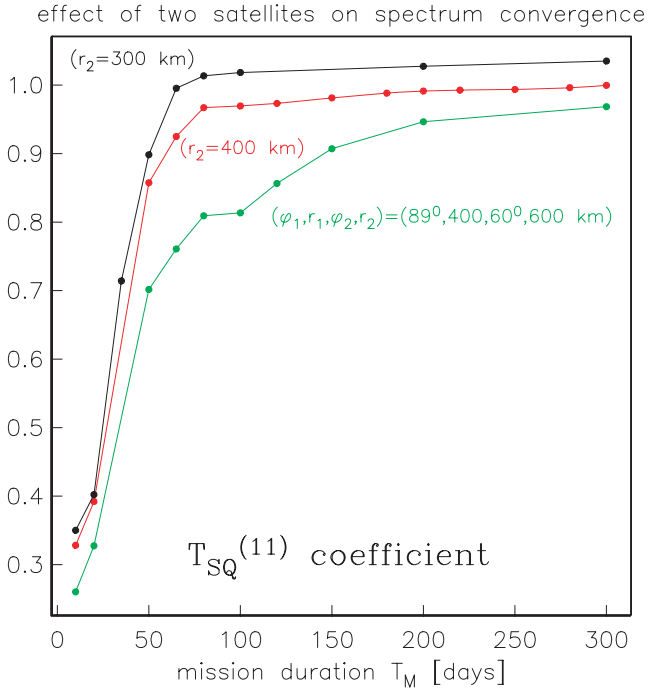

Figure 16. Effect on the SH spectral reconstruction of the geomagnetic T^{SQ} element of adding a second LEO satellite at various orbital radii.

conductivity variations could be extracted. Turner *et al.* (2007) have demonstrated the viability of constructing UT maps from champ Sq satellite induction signals.

Parametric studies of the Sq geomagnetic UT spectra have revealed several important results, which are strictly valid only for layered Earth conductivity models. First, a single LEO satellite should be in orbit for at least 1 yr under quiet conditions to ensure accurate reconstruction of a geomagnetic spectrum. Second, the length of the daily sampling window apparently does not have a major effect on spectral reconstruction. Third, the addition of random day-to-day variability in the Sq source strength also has little effect on the T^{SQ} spectral reconstruction. Fourth, geomagnetic spectral coefficients increase as mid-mantle conductivity increases although the shape of the spectra, and spectral ratios, remain fixed independent of mantle conductivity. Finally, in consideration of a multisatellite mission, with a first LEO satellite at canonical radius of 400 km and in near-polar orbit, a second LEO satellite is optimally inclined at $\sim 60^\circ$ and placed in a somewhat lower orbit. Further research employing 3-D forward modelling of induction in a laterally heterogeneous earth, with more realistic and complete external source descriptions, is required to test the robustness of these results.

Although satellites in LEO are presently mapping the geomagnetic field with increasing levels of fine detail, characterization of the external field plus its induced contribution remain largely uncertain. The main knowledge gaps are the complex spatiotemporal structure of the external ionospheric and magnetospheric sources and the heterogeneous electrical conductivity distribution within the Earth's crust and mantle. Eventually, LEO satellite induction signals can be inverted, along with ground observatory records, seismic data and other types of geological and geophysical information, to analyse deep-seated geological processes and map crust and mantle physiochemical properties such as fluid content and temperature.

ACKNOWLEDGMENTS

This research was put into sharper focus after discussions with Alexei Kuvshinov and Jakub Velímsky at the 2009 Swarm workshop in Potsdam. The author thanks the reviewers and editor Richard Holme for suggestions, which greatly improved the paper.

REFERENCES

Arfken, G.B. & Weber, H.J., 2005. *Mathematical Methods for Physicists,* 1200 pp., 6th edn, Academic Press, Burlington, MA.

Blakely, R.J., 1995. *Potential Theory in Gravity and Magnetic Applications,* 441 pp., Cambridge Univ. Press, Cambridge.

Campbell, W.H., 1989. The regular geomagnetic field variations during quiet solar conditions, in *Geomagnetism,* ed.Jacobs, J.A., Vol. 3, pp. 385–460, Academic Press, San Diego, CA.

Chen, G.X., Xu, W.Y., Du, A.M., Wu, Y.Y., Chen, B. & Liu, X.C., 2007. Statistical characteristics of the day–to–day variability in the geomagnetic Sq field, *J. geophys. Res.,* **112,** doi:10.1029/2006JA012059.

Everett, M.E., 2006. Local time stacking of geomagnetic solar daily variations, *J. geophys. Res.,* **111,** doi:10.1029/2005JB003831.

Fainberg, E.B., Kuvshinov, A.V. & Singer, B.Sh., 1990. Electromagnetic induction in a spherical earth with non-uniform oceans and continents in electric contact with the underlying medium–II. Bimodal global geomagnetic sounding of the lithosphere, *Geophys. J. Int.,* **102,** 283–286.

Grammatica, N. & Tarits, P., 2002. Contribution at satellite altitude of electromagnetically induced anomalies arising from a three-dimensional heterogeneously conducting Earth, using Sq as an inducing source field, *Geophys. J. Int.,* **151,** 913–923.

Healy, D.J., Jr., Rockmore, D.N., Kostolec, P.J. & Moore, S., 2003. FFTs for the 2-sphere: improvements and variations, *J. Fourier Anal. Appl.,* **9,** 340–385.

Kelbert, A., Schultz, A. & Egbert, G., 2009. Global electromagnetic induction constraints on transition: zone water contents, *Nature,* **460,** 1003–1005.

Kuvshinov, A., Manoj, C., Olsen, N. & Sabaka, T., 2007. On induction effects of geomagnetic daily variations from equatorial electrojet and solar quiet sources at low and middle latitudes, *J. geophys. Res.,* **112,** doi:10.1029/2007JB004955.

Macmillan, S. & Maus, S., 2005. International Geomagnetic Reference Field: the tenth generation, *Earth Planets Space,* **57,** 1135–1140.

Malin, S.R.C., 1973. Worldwide distribution of geomagnetic tides, *Phil. Trans. Royal Soc. London A,* **274,** 551–594.

Maus, S. *et al*., 2009. EMAG2: a 2–arc min resolution Earth Magnetic Anomaly Grid compiled from satellite, airborne and marine magnetic measurements, *Geochem. Geophys. Geosyst.,* **10,** doi:10.1029/2009GC002471.

Olsen, N., 1998. The electrical conductivity of the mantle beneath Europe derived from *c*–responses from 3 h to 720 h, *Geophys. J. Int.,* **133,** 298–308.

Olsen, N. *et al*., 2006. The Swarm End–to–End mission simulator study: a demonstration of separating the various contributions to Earth's magnetic field using synthetic data, *Earth Planets Space,* **58,** 359–370.

Olsen, N., Mandea, M., Sabaka, T. &Toffner-Clausen, L., 2009. CHAOS–2: a geomagnetic field model derived from one decade of continuous satellite data, *Geophys. J. Int.,* **179,** 1477–1487.

Sabaka, T.J., Olsen, N. & Langel, R.A., 2002. A comprehensive model of the quiet–time, near–Earth magnetic field: phase 3, *Geophys. J. Int.,* **151,** 32–68.

Sabaka, T.J., Olsen, N. & Purucker, M., 2004. Extending comprehensive models of the Earth's magnetic field with Oersted and CHAMP data, *Geophys. J. Int.,* **159,** 521–547.

Salby, M.L., 1982. Sampling theory for asynoptic satellite observations. Part I: space–time spectra, resolution, and aliasing, *J. Atmos. Sci.,* **39,** 2577–2600.

Sapozhnikov, A.B., Radugin, O.K. & Bobrova, M.N., 1969. Sphere in the field of a coil in an infinite conducting and magnetic medium, *Izvestiya Vyssch. Uch. Zaved. Fiz.,* **12,** 31–36. (Engl. transl.)

Schmucker, U., 1999a. A spherical harmonic analysis of solar daily variations in the years 1964–1965: response estimates and source fields for global induction–I. Methods, *Geophys. J. Int.,* **136,** 439–454.

Schmucker, U., 1999b. A spherical harmonic analysis of solar daily variations in the years 1964–1965: response estimates and source fields for global induction–II. Results, *Geophys. J. Int.,* **136,** 455–476.

Shin, K.S. & North, G.R., 1988. Sampling error study for rainfall estimate by satellite using a stochastic method, *J. appl. Meteor.,* **27,** 1218–1231.

Stening, R., Reztsova, T. & Minh, L.H., 2005. Day–to–day changes in the latitudes of the foci of the Sq current system and their relation to equatorial electrojet strength, *J. geophys. Res.,* **110,** doi:10.1029/2005JA011219.

Stratton, J.A., 1941. *Electromagnetic Theory,* McGraw Hill, New York, NY, 414ff.

Sugiura, M., 1964. Hourly values of equatorial Dst for IGY, *Annals Intl. Geophys. Year,* **35,** 945–948.

Turner, J.P.R., Winch, D.E., Ivers, D.J. & Stening, R.J., 2007. Regular daily variations in satellite magnetic total intensity data, *Ann. Geophys.,* **25,** 2167–2174.

Velímsky, J. & Everett, M.E., 2005. Electromagnetic induction by Sq ionospheric currents in a heterogeneous Earth: modeling using ground–based and satellite measurements, in *Earth Observation with CHAMP: Results From Three Years in Orbit,* eds Reigber, C., Lühr, H., Schwintzer, P. & Wickert, J., pp. 341–346, Springer, Berlin.

Velímsky, J. & Martinec, Z., 2005. Time-domain, spherical harmonic-finite element approach to transient three-dimensional geomagnetic induction in a spherical heterogeneous Earth, *Geophys. J. Int.,* **161,** 81–101.

Willis, N.P. & Bresler, Y., 1997. Lattice–theoretic analysis of time–sequential sampling of spatiotemporal signals—Part I, *IEEE Trans. Info. Theory,* **43,** 190–207.

Winch, D.E., 1981. Spherical harmonic analysis of geomagnetic tides, 1964–1965, *Phil. Trans. Royal Soc. London A,* **303,** 1–104.

APPENDIX A: LEO SATELLITE ORBIT

Formulae for a circular LEO satellite trajectory $\{\phi(t), \lambda(t)\}$, where ϕ is latitude and λ is longitude, are given in Shin & North (1988). They are

$$\phi(t) = \sin^{-1}\{\sin\Psi \sin([\Theta + \gamma]\, t)\}; \tag{A1}$$

$$\lambda(t) = \tan^{-1}\{\cos\Psi \tan([\Theta + \gamma]\, t)\} - (\Omega - \alpha_p)\, t. \tag{A2}$$

In the above equations, Ψ is the satellite inclination, γ is the angular velocity of precession of the satellite in its orbital plane, α_p is the angular velocity of precession on the equatorial plane due to Earth's oblateness, $\Omega = 7.2921159\times10^{-5}$ rad s^{-1} is Earth's angular velocity on the equatorial plane, and t is time. The parameter Θ in eqs (A1, A2) is

$$\Theta = \sqrt{\frac{\gamma}{r^3}}\left[1 + \frac{3}{2}J_2\frac{r_E^2}{r^2}\sqrt{1-\varepsilon^2}\left(1 - \frac{3}{2}\sin^2\Psi\right)\right]; \tag{A3}$$

where $\gamma = 398\,601.2$ km^3 s^{-2} is the gravitational constant, $r_E = 6371.0$ km is the Earth mean radius, $r = r_E + h$ is the satellite orbit radius with h the satellite altitude, ε is the orbital eccentricity ($\varepsilon = 0$ for a circular orbit), and $3J_2/2 = 1.6238235\times10^{-3}$. The angular velocities of precession are given by

$$\gamma = \frac{3}{2}J_2\frac{r_E^2}{r^2}\Theta\left(2 - \frac{5}{2}\sin^2\Psi\right); \tag{A4}$$

$$\alpha_p = -\frac{3}{2}J_2\frac{r_E^2}{r^2}\Theta\cos\Psi. \tag{A5}$$

APPENDIX B: SH TRANSFORM

Consider the SH expansion of an arbitrary function $f(\theta, \phi)$,

$$f(\theta,\phi)=\sum_{n\geq 0}\sum_{|m|\leq n}\overline{f}_{nm}q_{nm}P_{nm}(\cos\theta)\exp(im\phi), \tag{B1}$$

with normalizing coefficients (Arfken & Weber 2005)

$$q_{nm}=\sqrt{\frac{2n+1}{4\pi}\frac{(n-m)!}{(n+m)!}}. \tag{B2}$$

The SH transform determines the coefficients $\overline{f}_{nm}$ of a function $f(\theta, \phi)$ that is evenly sampled at the colatitude θ and longitude ϕ gridpoints

$$\theta_j=\frac{\pi(2j+1)}{4B};\quad \phi_k=\frac{\pi k}{B}; \tag{B3}$$

for $j, k = 1, \ldots, 2B–1$. Healy *et al.* (2003) have shown that

$$\overline{f}_{nm}=\frac{\sqrt{2\pi}}{2B}\sum_{j=0}^{2B-1}\sum_{k=0}^{2B-1}a_j^{(B)}f(\theta_j,\phi_k)q_{nm}P_{nm}(\cos\theta_j)\times\exp(-im\phi_k), \tag{B4}$$

where the weighting coefficients are given by

$$a_j^{(B)}=\sqrt{\frac{2\pi}{B}}\sin\left(\frac{\pi\left[j+1/2\right]}{2B}\right)\times\sum_{l=0}^{B-1}\frac{1}{2l+1}\sin\left(\frac{[2l+1]\pi\left[j+1/2\right]}{2B}\right). \tag{B5}$$

The formula (B4) is used in this paper to evaluate SH spectra of the sampled Sq geomagnetic field.

APPENDIX C: DERIVATION OF $\mathbf{B}^{SQ}$ AT LEO SATELLITE ALTITUDE

Here we derive the Sq geomagnetic field $\mathbf{B}^{SQ}$ that would be measured at LEO satellite altitude, above the ionosphere, for a layered conducting Earth with radius b_1 and radial conductivity profile $\sigma(r)$. The field $\mathbf{B}^{SQ}$ is excited by a source electric current $\mathbf{K}$ of prescribed (n, m) SH spatial structure and frequency $\omega_p = 2\pi p$ rad d^{-1}. The source current flow is confined to an infinitesimally thin spherical shell at radius $r = a$, which represents the ionosphere. Induced currents in the Earth are responsible for a secondary contribution to $\mathbf{B}^{SQ}$.

The geomagnetic potential $U(\mathbf{r})$ in the geospace region $r > a$ external to the ionosphere may be expanded into a series of spatiotemporal SHs as (Schmucker 1999a; Sabaka *et al.* 2002; Velímsk & Everett 2005)

$$U(r,\theta,\phi)=a\sum_{p=1}^{P}\sum_{m=p-M}^{p+M}\sum_{n=m}^{m+N-1}U_{nmp}\left(\frac{a}{r}\right)^{n+1}\times P_{nm}(\cos\theta)\exp(im\phi)\exp(i\omega_p t), \tag{C1}$$

where U_{nmp} is the contribution of spatiotemporal mode (n, m, p) and P_{nm} are the associated Legendre functions, as defined in Arfken & Weber (2005). The highest order mode in the expansion is determined by the truncation level (N, M, P). In eq. (C1), diurnal variations are included but seasonal variation has been neglected.

The geomagnetic potential $V(\mathbf{r})$ in the atmosphere region $b_1 < r < a$ is similarly expanded as

$$V(\mathbf{r})=\sum_{pmn}\left[b_1V_{nmp}\left(\frac{b_1}{r}\right)^{n+1}+a\overline{V}_{nmp}\left(\frac{r}{a}\right)^{n}\right]P_{nm}(\cos\theta)\times\exp(im\phi)\exp\left(i\omega_p t\right) \tag{C2}$$

where $\overline{V}_{nmp}$ is the contribution of mode (n, m, p) to the geomagnetic potential in the atmosphere caused by current flow in the overlying ionosphere, while V_{nmp} is the contribution caused by induced current flow inside the underlying Earth. The summation in (C2) over the n, m, p indices is the same as in eq. (C1).

In this paper we restrict time variations to the diurnal $p = 1$ and semidiurnal $p = 2$ modes and henceforth drop the explicit $\exp(i\omega_p t)$ time dependence and set $\omega = \omega_p$. Later papers will consider higher order temporal modes. The Earth is assumed herein to consist of radial layers such that electrical conductivity is uniform within each of N layers.

The magnetic field $\mathbf{H}^{(i)}$ inside the ith radial layer of the Earth obeys the Helmholtz diffusion equation

$$\nabla^2\mathbf{H}^{(i)}-\beta_i^2\mathbf{H}^{(i)}=0; \tag{C3}$$

where $\beta_i=\sqrt{i\mu_0\sigma_1\omega}$. The magnetic field $\mathbf{H}^{(i)}$ can be expanded into a series of vector SHs (Stratton 1941) as

$$\mathbf{H}^{(i)}=\frac{\beta_i}{i\omega\mu_0}\sum_{nm}A_{nm}^{(i)}\mathbf{M}_{nm}^{(i)}+B_{nm}^{(i)}\mathbf{N}_{nm}^{(i)}, \tag{C4}$$

where $\mathbf{M}_{nm}^{(i)}=\nabla\times\mathbf{r}\psi_{nm}^{(i)}$ and $\mathbf{N}_{nm}^{(i)}=\frac{1}{\beta_i}\nabla\times\mathbf{M}_{nm}^{(i)}$. The eigenfunctions $\psi_{nm}^{(i)}$ are solutions to the scalar Helmholtz diffusion equation $\nabla^2\psi_{nm}^{(i)}-\beta_i^2\psi_{nm}^{(i)}=0$, that is

$$\psi_{nm}^{(i)}=\left\{\begin{array}{c}\iota_n(\beta_i r)\\ \kappa_n(\beta_i r)\end{array}\right\}P_{nm}(\cos\theta)\exp(im\phi); \tag{C5}$$

where the spherical 'modified' Bessel functions $\iota_n(\beta_i r)$ and $\kappa_n(\beta_i r)$ are the appropriate solutions for this diffusion problem (Arfken & Weber 2005). Use of the spherical Bessel and Hankel functions (e.g. Sapozhnikov *et al.* 1969) is also possible in eq. (C5) but they are oscillatory and ill suited for numerical computations.

The radial and polar components of eq. (C4) are easily found,

$$H_r^{(i)}=\frac{1}{i\omega\mu_0 r}\sum_{nm}B_{nm}^{(i)}n(n+1)\psi_{nm}; \tag{C6}$$

$$H_\theta^{(i)}=\frac{1}{i\omega\mu_0 r}\sum_{nm}B_{nm}^{(i)}\frac{\partial^2}{\partial r\partial\theta}(r\psi_{nm}). \tag{C7}$$

The coefficients A_{nm} in eq. (C4) vanish upon application of boundary conditions appropriate for induction in a radial earth by an external source and hence the terms involving vector SH $\mathbf{M}_{nm}$ are excluded from eqs (C6) and (C7). In terms of the spherical modified Bessel functions these equations become

$$H_r^{(i)}=\frac{1}{i\omega\mu_0 r}\sum_{nm}n(n+1)P_{nm}(\cos\theta)\times\exp(im\phi)\left[T_{nm}^{(i)}\iota_n(\beta_i r)+\overline{T}_{nm}^{(i)}\kappa_n(\beta_i r)\right]; \tag{C8}$$

$$H_\theta^{(i)}=\frac{1}{i\omega\mu_0 r}\sum_{nm}\frac{\partial P_{nm}}{\partial\theta}\exp(im\phi)\left[T_{nm}^{(i)}\lambda_n(\beta_i r)+\overline{T}_{nm}^{(i)}\mu_n(\beta_i r)\right]; \tag{C9}$$

where

$$\lambda_n(\beta_i r) = \frac{\partial}{\partial r}\left[r\iota_n(\beta_i r)\right] \text{ and } \mu_n(\beta_i r) = \frac{\partial}{\partial r}\left[r k_n(\beta_i r)\right]. \quad \text{(C10)}$$

The unknown coefficients in eqs (C1, C2, C8, C9) are found by enforcing continuity of the radial and polar magnetic field at each of the internal boundaries inside the Earth. It is also required to set the magnetic field to zero at the centre of the Earth ($r = 0$). On the surface of the Earth $r = b_1$, the relevant boundary conditions are $H_r^{(1)} = -\partial V/\partial r$ and $H_\theta^{(1)} = -(1/r)\partial V/\partial\theta$.

To connect the ionospheric electric current source to the geomagnetic potentials, we define an equivalent current function $\Phi = \Phi(\theta,\phi)$ such that the current density $\mathbf{K}$ at the ionosphere $r = a$ is

$$\mathbf{K} = \hat{\mathbf{r}} \times \nabla\Phi. \quad \text{(C11)}$$

The equivalent current function Φ in the ionosphere is expanded in spatiotemporal SHs as

$$\Phi(\theta, \phi) = \sum_{nm} C_{nm} P_{nm}(\cos\theta) \exp(im\phi). \quad \text{(C12)}$$

The function Φ in eq. (C12) acts as the source term driving the Sq geomagnetic field $\mathbf{B}^{\mathrm{SQ}}$. From eq. (C11) the ionospheric current density $\mathbf{K}$ is

$$\mathbf{K} = \sum_{nm} \hat{\phi}\frac{C_{nm}}{r}\frac{\partial P_{nm}}{\partial\theta}\exp(im\phi) - \hat{\theta}\frac{imC_{nm}}{r\sin\theta}P_{nm}\exp(im\phi). \quad \text{(C13)}$$

The boundary conditions on the tangential components of the magnetic field $\mathbf{H}$ are

$$\hat{\mathbf{r}} \times (H^{\mathrm{AIR}} - H^{\mathrm{SPACE}}) = K \, at \, r = a, \quad \text{(C14)}$$

which, using the definition of the magnetic field in terms of the negative gradient of the geomagnetic potential V in the air region and U in the space region, becomes

$$\hat{\mathbf{r}} \times (-\nabla V + \nabla U) = \hat{\mathbf{r}} \times \nabla\Phi \text{ at } r = a. \quad \text{(C15)}$$

From eq. (C15) it follows immediately that $U–V = \Phi$, which states that the equivalent current function $\hat{\mathbf{r}}$ equals the jump in the potential across the ionosphere. Continuity of the radial magnetic field $\mathbf{H}$ across the ionosphere provides the boundary condition

$$\frac{\partial V}{\partial r} = \frac{\partial U}{\partial r} \text{ at } r = a. \quad \text{(C16)}$$

The tangential θ component of eq. (C15) is

$$\frac{\partial U}{\partial\theta} - \frac{\partial V}{\partial\theta} = \frac{\partial\Phi}{\partial\theta} \text{ at } r = a, \quad \text{(C17)}$$

which is a second boundary condition on U and V.

The application of the boundary conditions produces a linear system of equations in the unknown coefficients for the specified values of the degree n, order m, and strength C_{nm} of the equivalent current function Φ in the ionosphere. Note that the SH degrees and orders (n, m) decouple for a 1-D earth in which $\sigma = \sigma(r)$, such that a given degree and order (n, m) for the current function Φ generates only coefficients of the same degree and order. A more general Earth conductivity function $\sigma = \sigma(r, \theta, \phi)$ would generate coefficients of many different pairs (n, m) of degrees and orders. This more difficult case is not considered in this paper.

Once the unknown coefficients are determined, the magnetic field $\mathbf{B}^{\mathrm{SQ}}$ at LEO satellite altitude in the space region $r > a$ above the ionosphere is found using

$$\mathbf{B}^{\mathrm{SQ}} = -\mu_0\nabla U; \quad \text{(C18)}$$

where U is given by eq. (C1).